Materials Letters 338 (2023) 133975

Contents lists available at ScienceDirect

Materials Letters

journal homepage: www.elsevier.com/locate/matlet

On the use of microwaves during combustion/calcination of *N*-doped TiO_2 precursor: An EMW absorption study combined with TGA-DSC-FTIR results

Enrico Paradisi [a], Pedro J. Plaza-González [b], Giovanni Baldi [c], José M. Catalá-Civera [b], Cristina Leonelli [a,*]

[a] Department of Engineering "Enzo Ferrari", University of Modena and Reggio Emilia, Via Pietro Vivarelli 10, 41125 Modena, Italy
[b] Microwave Division (DiMaS), ITACA Research Institute, Universitat Politècnica de València, Camino de Vera, 46022 Valencia, Spain
[c] Ce.Ri.Col. Colorobbia Research Centre, Colorobbia Consulting S.R.L., Via Pietramarina, 123, 50053 Sovigliana-Vinci (Fi), Italy

ARTICLE INFO

Keywords:
N-doped titania
Thermal analysis
Evolved gas analysis
Microwave irradiation
Dielectric properties
Cavity perturbation method

ABSTRACT

For the first time, dielectric properties and electromagnetic wave (EMW) absorbing performance of a precursor for *N*-doped TiO_2 nanoparticles undergoing combustion synthesis are reported. The precursor contains titania, NH_4Cl as source of N atoms for TiO_2 nanoparticles doping, and organics. Thermogravimetric analysis (TGA) reveals that the 180–450 °C temperature range accounts for the overall weight loss of the process. High-temperature gas evolution analysis confirms combustion of the organic component. Aiming to optimize output power and time schedule of the material's microwave (MW) calcination, *in situ* high temperature dielectric properties measurements were recorded during MW irradiation in a dedicated cavity. Results revealed that after a first stage of non-combustive decomposition, in a second stage the EMW absorption decreases, so MW power is no longer necessary and hybrid heating is suggested to reach the desired calcination temperature (375–400 °C).

1. Introduction

The introduction of nitrogen as TiO_2 dopant is an excellent method to improve photocatalytic performance of titania under visible light [1]. This requires a controlled entrapment of N atoms and an optimized mix of TiO_2 crystalline phases [2]. A common method for N-TiO_2 doping is the calcination of a precursor containing *N*-bearing compounds [3]. In our case, the N-TiO_2 precursor contains TiO_2, NH_4Cl and citrate derivatives, the latter to be removed during calcination at 400 °C, contemporarily to TiO_2 doping with nitrogen. The final product should contain mainly anatase and a minor fraction of rutile.

While using microwave irradiation at 2.45 GHz to sustain this calcination, we encountered a serious reproducibility problem, obtaining very different phase compositions in several tests performed in the same conditions. Wondering if this could be due to an intense change in MW absorption at high temperatures, an EMW absorption test for *in situ* high temperature monitoring of the dielectric properties of the system was set up.

Being this test accessible only in few laboratories [4–5], the cavity perturbation technique with visual control of the sample transformation is perfectly suitable to investigate the material's behaviour during heating [6–7] and is the only one able to measure MW absorption at such high temperatures.

While MW-assisted ignition of self-supported high temperature syntheses (SHS) are widespread [8], only few reports are available on MW combustion syntheses (CS). Anyway, we believe that it is crucial to know at which actual specimen's temperature the electromagnetic energy is better absorbed by the sample during MW calcination, to modulate MW power during the process for energy optimization and fine tuning of material's properties.

In this work we present thermal and dielectric behaviour of our precursor during calcination using TGA-DSC-FTIR and EMW absorbance measurements.

2. Materials and methods

The *N*-doped titania precursor is synthesized in an acidic environment (HCl), then pH is neutralized with ammonium citrate dibasic to form a mixture of TiO_2, NH_4Cl and citrate salts [9]. All the by-products are then removed by calcination, typically at 400 °C in a conventionally

* Corresponding author.
E-mail addresses: enrico.paradisi@unimore.it (E. Paradisi), pedplago@itaca.upv.es (P.J. Plaza-González), baldig@colorobbia.it (G. Baldi), jmcatala@dcom.upv.es (J.M. Catalá-Civera), cristina.leonelli@unimore.it (C. Leonelli).

https://doi.org/10.1016/j.matlet.2023.133975
Received 12 August 2022; Received in revised form 19 January 2023; Accepted 27 January 2023
Available online 30 January 2023

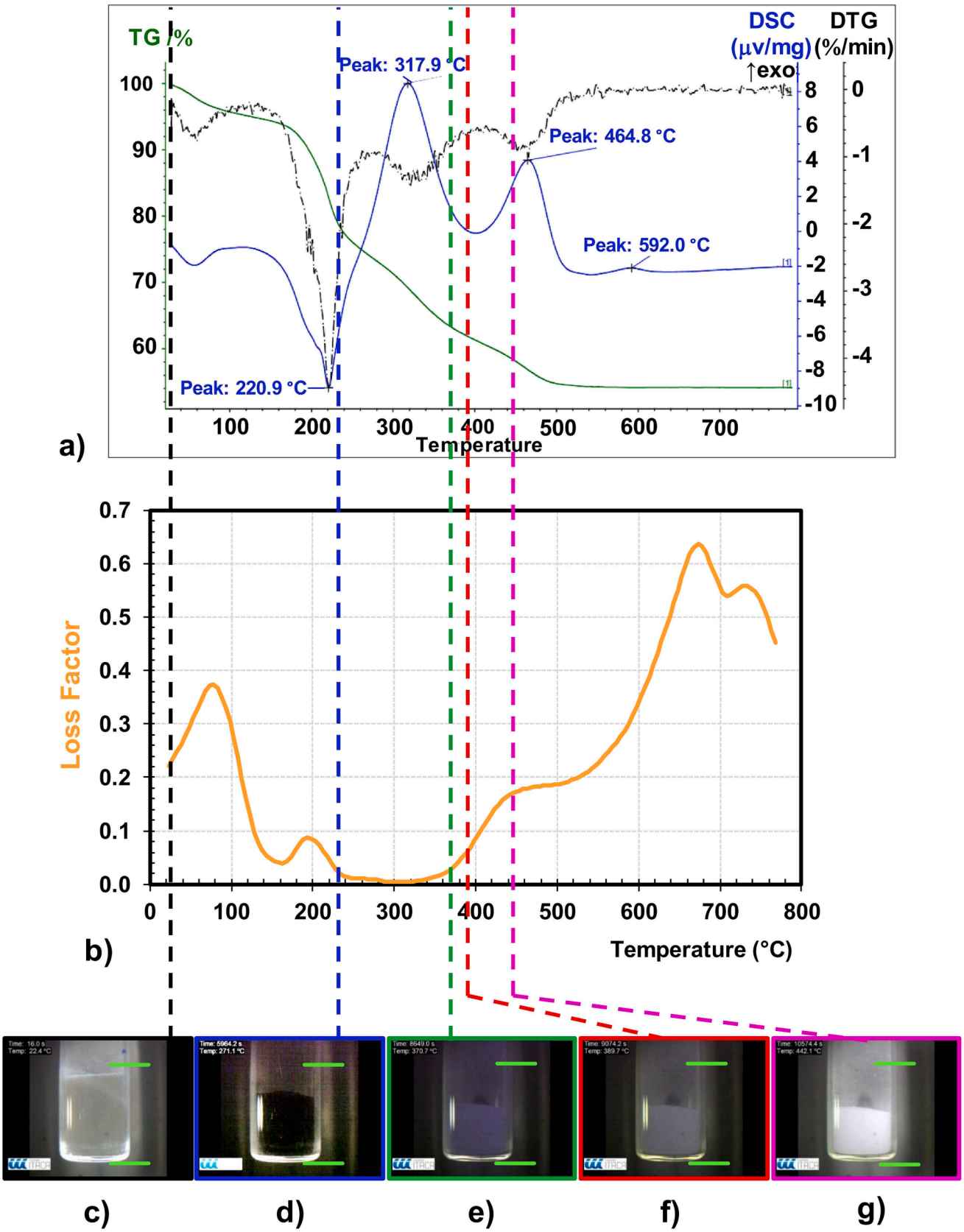

Fig. 1. **(a):** TGA/DSC curve for the *N*-doped TiO_2 precursor between r.t. and 800 °C: TGA (green curve), first derivative DTG (dashed black), and DSC (blue). **(b):** loss factor trend increasing temperature. **(c)-(g):** sample's photographs at different temperatures. **(c):** 22 °C, **(d):** 230 °C, **(e):** 370 °C, **(f):** 389 °C, **(g):** 442 °C.

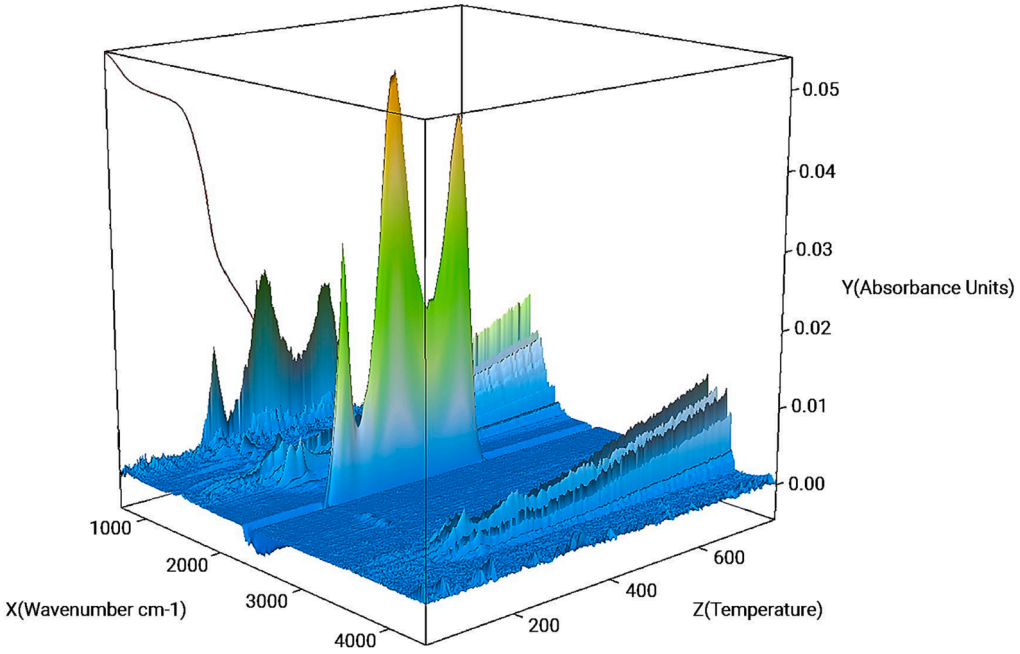

Fig. 2. 3D image of FTIR spectrum from 500 to 4500 cm^{-1} showing gaseous molecules evolved over a temperature range up to 800 °C.

heated oven [10]. We performed the same calcination in a MW muffle furnace (Phoenix Black, CEM Matthews, NC, USA) but the obtained results were not reproducible, varying a lot even if performed in the same conditions. Details about the synthesis, calcination and material's properties are given in the *supporting information*.

TGA-DSC-FTIR analysis was performed on titania precursor at 10 °C/min in a Netzsch STA 449F3 instrument coupled with evolved gas analysis via Bruker FT-IR spectrometer.

The MW absorption of this material was tested from room temperature till 800 °C using the cavity perturbation method (CPM). In this method, 0.5 g of precursor were introduced inside a quartz vial (height: 15 mm, diameter: 9.8 mm) which was placed in a cavity where microwave heating and simultaneous measuring of dielectric properties is feasible with two different sources without interference [11]. Sample's temperature is measured by an external IR pyrometer pointing to the surface of the quartz holder. Extensive calibration procedures are applied to determine the sample's bulk temperature from the pyrometer measurement [7].

3. Results and discussion

3.1. TGA-DSC-FTIR results

The precursor's TGA-DSC graphic (Fig. 1**(a)**) shows two main endothermic peaks (~70 °C and ~221 °C) and three main exothermic peaks (317.9 °C, 494.8 °C, 592 °C), all but the last one associated to weight loss. The first two endothermic peaks correspond to water loss and to citrate decarboxylation [12]. The first two exothermic peaks correspond to further citrate derivatives decomposition, while the last one is given by the anatase–rutile transformation [13]. Weight loss (45%) causes a drastic volume reduction as visualized by the level indicators at the right of the quartz tube (Fig. 1**(c)-(g),** green lines). Such change in the sample's geometry affects the EMW absorption as well as the changes in chemical composition (see details in section 3.2).

Fig. 2 shows the 3D image of the FTIR spectra of the gases evolved by the sample at different temperatures, with the TGA trace at the rear. The most intense signals are observed from 200 °C in correspondence with the first (endothermic) decomposition peak and are located at ~ 2360 and ~ 660 cm^{-1}. These signals are observed up to ~ 500 °C and three maxima of gas evolution are observed at the same temperatures of the three main decompositions in DSC. Other major signals emerge from 200 °C at 1300–2000 cm^{-1} and 3500–4000 cm^{-1}, continuously increasing in intensity. These two sets of signals belong to CO_2 and water [14], confirming citrate decarboxylation and combustion [12].

Other small peaks emerge in the 2D spectrum recorded at 220 °C (Fig. 3**(a)**) at 889, 977, 1250 and 1792 cm^{-1} (red circles). Since the region around 1800 cm^{-1} typically shows anhydride C═O stretching, these peaks might belong to citraconic anhydride [15], a known citric acid decomposition product, obtained after water loss and decarboxylation [12]. Citraconic anhydride should boil just after its formation (213–214 °C [15]), partly explaining why the main peak at 220 °C is endothermic in DSC.

A small amount of HCl can also be seen in this spectrum (blue circled) [16]. We suppose that NH_4Cl decomposition occurs around this temperature (220 °C), to give free NH_3 and HCl despite this event should occur later [17]. Indeed, during calcination a white solid crystallizes on the cooling pipe's walls around that temperature, and reasonably this compound cannot be anything else except NH_4Cl re-crystallizing on cool walls after high temperature decomposition inside the oven. The presence of NH_3 and HCl is not evident in our spectra (especially NH_3), but it is known that their IR signals might not be detected at low concentration in the gas phase when CO_2 and water are also present in the mixture [18].

The FTIR spectrum recorded at 324 °C (Fig. 3**(b)**), along with CO_2 and water, shows the presence of CO in small amounts (green circle in Fig. 3**(b)**) [14]. CO is not detected in the spectrum recorded at 462 °C (Fig. 3**(c)**), while CO_2 and water are still present. These events indicate that the remaining organics undergo an exothermic combustion reaction as temperature increases in the range 250–450 °C (compare with Fig. 1 **(a)**).

Water detection above 500 °C in the 3D FTIR spectrum (Fig. 2), can be explained by an augmented moisture presence in the instrument or by TiO_2 nanoparticles growth through dehydration mechanism [19].

3.2. EMW results

The curve of loss factor (ε″), the imaginary component of permittivity, shows higher values below 250 °C and above 400 °C (Fig. 1**b**), but

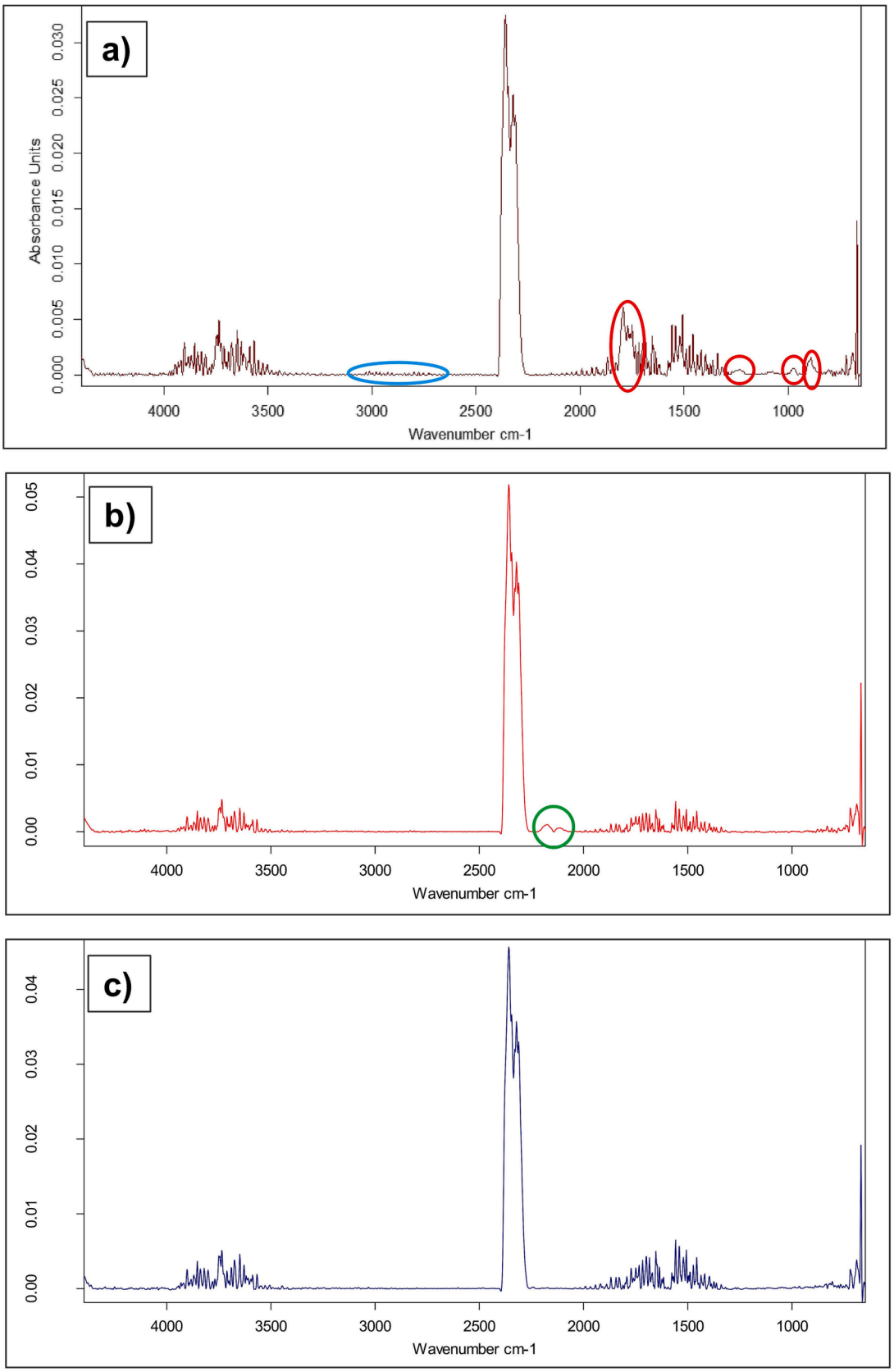

Fig. 3. FTIR Spectrum of gas evolved at **(a)** 220 °C, **(b)** 324 °C and **(c)** 462 °C.

is almost equal to zero between 250 °C and 400 °C. This means that in that temperature range the sample is not able to convert MW energy into heat, since this ability is given by tan δ = ε"/ε' which is obviously = 0 if ε" = 0 [8]. Thus, considering the previous discussion of TGA-DSC-FTIR results, MW heating is active only during the endothermic decarboxylation and NH_4Cl decomposition, and later, when rutile is formed, but is not active during the main combustion (compare Fig. 1**(b) and 1(a)**). This means that the process is a self-supported combustion and MW heating is not necessary in that stage.

4. Conclusions

The scarce reproducibility of calcination's outcome is not due to an abnormal material's MW absorption during heating, but it is solely due to the well-known combustion unpredictability. Therefore, other parameters (i.e. oxygen amount or heating rate) should be investigated for a better control on the calcination's outcome. Anyway, another meaningful conclusion of this work is that, during combustion, MW energy application is not needed, and this calcination is better performed using hybrid heating.

This paper shows that accurate study of thermal events combined with EMW absorption measurements is a powerful way to understand how to modulate MW power during MW-assisted calcinations avoiding unnecessary energy consumption.

CRediT authorship contribution statement

Enrico Paradisi: Methodology, Investigation, Writing – original draft. **Pedro J. Plaza-González:** Investigation, Data curation, Visualization. **Giovanni Baldi:** Conceptualization. **José M. Catalá-Civera:** Visualization, Writing – original draft. **Cristina Leonelli:** Supervision, Conceptualization, Writing – review & editing.

Declaration of Competing Interest

The authors declare that they have no known competing financial interests or personal relationships that could have appeared to influence the work reported in this paper.

Data availability

Data will be made available on request.

Acknowledgements

Authors are grateful to Paola Miselli, Paolo Pozzi and Cristina Siligardi for supporting with the TGA/EGA analysis.

Funding

This work was carried out within the European project: "Sonication and Microwave Processing of Material Feedstock (SIMPLIFY)" supported by the European Union's Horizon 2020 research and innovation program under Grant Agreement No 820716.

Appendix A. Supplementary data

Supplementary data to this article can be found online at https://doi.org/10.1016/j.matlet.2023.133975.

References

[1] R. Asahi, T. Morikawa, H. Irie, T. Ohwaki, Chem. Rev. 114 (2014) 9824–9852, https://doi.org/10.1021/cr5000738.
[2] J. Lynch, C. Giannini, J.K. Cooper, A. Loiudice, I.D. Sharp, R. Buonsanti, J. Phys. Chem. C 119 (13) (2015) 7443–7452, https://doi.org/10.1021/jp512775s.
[3] H. Yu, X. Zheng, Z. Yin, F. Tao, B. Fang, K. Hou, Chin. J. Chem. Eng. 15 (6) (2007) 802–807, https://doi.org/10.1016/S1004-9541(08)60006-3.
[4] M. Dietrich, D. Rauch, A. Porch, R. Moos, Sensors (Switzerland) 14 (9) (2014) 16856–16868, https://doi.org/10.3390/s140916856.
[5] M.J. Kamaruddin, N.T. Nguyen, G.A. Dimitrakis, J. El Harfi, E.R. Binner, S. W. Kingman, E. Lester, J.P. Robinson, D.J. Irvine, RSC Adv. 4 (11) (2014) 5709–5717, https://doi.org/10.1039/C3RA46941G.
[6] B. Garcia-Baños, J.M. Catalá-Civera, F.L. Peñaranda-Foix, P. Plaza-González, G. Llorens-Vallés, Materials 9 (5) (2016) 349, https://doi.org/10.3390/ma9050349.
[7] B. García-Baños, J.J. Reinosa, F.L. Peñaranda-Foix, J.F. Fernández, J.M. Catalá-Civera, Sci. Rep. 9 (2019) 10809, https://doi.org/10.1038/s41598-019-47296-0.
[8] R. Rosa, P. Veronesi, C. Leonelli, Chem. Eng. Process. 71 (2013) 2–18, https://doi.org/10.1016/j.cep.2013.02.007.
[9] G. Baldi, M. Bitossi, A. Barzanti, International Patent WO 2007/088151, August 9, 2007 [Colorobbia Italia S.p.A.].
[10] G. Baldi, L. Niccolai, M. Bitossi, V. Dami, A. Cioni, International Patent WO 2019/211787 A1. November 1, 2019 [Colorobbia Consulting S.R.L.].
[11] J.M. Catalá-Civera, A.J. Canós, P. Plaza-González, J.D. Gutiérrez, B. García-Baños, F.L. Peñaranda-Foix, IEEE Trans. Microw. Theory Techn. 63 (9) (2015) 2905–2914, https://doi.org/10.1109/TMTT.2015.2453263.
[12] K. Van Werde, D. Mondelaers, G. Vanhoyland, D. Nelis, M.K. Van Bael, J. Mullens, L.C. Van Poucke, B. Van Der Veken, H.O. Desseyn, J. Mater. Sci. 37 (2002) 81–88, https://doi.org/10.1023/A:1013141723764.
[13] X. Wen, S. Zhao, S. Asuha, J. Nanomater. 2019 (2019) 6467107, https://doi.org/10.1155/2019/6467107.
[14] N.H. Giron, M.C. Celina, Polym. Degrad. Stab. 145 (2017) 93–101, https://doi.org/10.1016/j.polymdegradstab.2017.05.013.
[15] https://spectrabase.com/spectrum/DpfnGmaCbis, 1980 (accessed 29/12/2022).
[16] https://spectrabase.com/spectrum/A4RitqnxEpp, 2021 (accessed 29/12/2022).
[17] B.B. Tatykaev, M.M. Burkitbayev, B.M. Uralbekov, F.K. Urakaev, Acta Phis. Pol. A 126 (4) (2014) 1044–1048, https://doi.org/10.12693/APhysPolA.126.1044.
[18] A.M. Giovannozzi, F. Pennecchi, P. Muller, P. Balma Tivola, S. Roncari, A.M. Rossi, Anal. Bioanal. Chem. 407 (2015) 8423–8431, https://doi.org/10.1007/s00216-015-9030-6.
[19] J. Chae, M. Kang, J. Power Sources 196 (2011) 4143–4151, https://doi.org/10.1016/j.jpowsour.2010.12.109.